Validation of a Computational Model of Cardiac Defibrillation

Jean Bragard[1], Jorge Elorza[1], Elizabeth M Cherry[2], Flavio H Fenton[3]

[1] Universidad de Navarra, Pamplona, Spain
[2] Rochester Institute of Technology, Rochester, NY, USA
[3] Georgia Institute of Technology, Atlanta, GA, USA

Abstract

We develop and validate a three-dimensional model of ventricular fibrillation for use in studying defibrillation. Specifically, we use a rabbit ventricular geometry as a realistic model system for evaluating the efficacy of defibrillatory shocks. Data obtained from the simulations are analyzed in terms of a dose-response curve. In agreement with clinically relevant values, we find that an electric field strength of about 6.6 V/cm indicates a 50% probability of successful defibrillation for a 12-ms monophasic shock in our model. Our validated model will be useful for optimizing defibrillation protocols and for performing detailed studies of defibrillation mechanisms.

1. Introduction

Ventricular fibrillation (VF) is a serious medical condition that requires immediate intervention. During VF, the electrical activity of the heart is disorganized, leading to localized and ineffective contraction that renders the heart unable to pump blood properly. Cardiac defibrillation [1] consists in the application of a very strong electric shock to restore the correct function of the heart. Unfortunately, defibrillation is not always successful. Computational studies can help to elucidate the mechanisms underlying defibrillation [2]. In this study, we construct a realistic model of the electrical activity inside the ventricles of the heart. To validate the model, we test the efficacy of defibrillation for different shock strengths and compare the success rate with available data from the literature.

The numerical model contains two primary fields, the extracellular and intracellular electric potentials. These fields are governed by partial differential equations that must be solved simultaneously (one is a stiff reaction-diffusion equation and the other is the Poisson equation). In Section 2, we discuss the basic equations that govern the problem and briefly outline the algorithm used to solve these equations efficiently. In particular, the equations are solved in parallel with the help of the PETSc package [3]. In Section 3, we analyze the results of the application of strong electric shocks using several initial conditions. From these results, it is possible to determine the energy needed for successful defibrilation. In the conclusions, we suggest directions for future studies aimed at designing milder defibrillatory shocks.

2. Model

The most commonly used model to describe the electrical activity of the heart during defibrillation is the bidomain model. The two fundamental fields of these equations are the intracellular electrical potential ϕ_i and the extracellular electrical potential ϕ_e. The two can be combined to write the transmembrane potential $V = \phi_i - \phi_e$, which is the quantity most accessible for direct experimental measurement in cardiac tissue.

2.1. Bidomain model

The complete mathematical expressions for the model are as follows [4]:

$$\frac{\partial s}{\partial t} = f(V, s) \tag{1}$$

$$\frac{\partial V}{\partial t} + I_m = \nabla \cdot (D_i \nabla V) + \nabla \cdot (D_i \nabla \phi_e) \tag{2}$$

$$\nabla \cdot ((D_i + D_e)\nabla \phi_e) = -\nabla \cdot (D_i \nabla V) - I_{ext} \tag{3}$$

where s is a state vector that contains all the variables associated with the description of ionic currents across the membrane, where all ion transport takes place. The mathematical description of the opening and closing of the ion channels is described by a set of differential equations (1). The time scales associated with these equations vary from 0.1 ms up to 1 s and higher. Furthermore, the vector function $f(V, s)$ in Eq. (1) is highly nonlinear. Consequently, the equations are stiff and are challenging to solve from the numerical point of view. Typical values for the conductivities [5] are $D_\parallel^{(i)} = 10^{-3}$, $D_\perp^{(i)} = 6.75 \text{x} 10^{-5}$, $D_\parallel^{(e)} = 1.5 \text{x} 10^{-3}$, and $D_\perp^{(e)} = 1.575 \text{x} 10^{-4}$, all in units of cm^2/ms; these correspond to the orthotropic tensors (D_i and D_e)

[4]. The large difference between the conductivities along the fibers ($\parallel$) and perpendicular to the fibers ($\perp$) allows for a significant difference in the speed of electrical wave propagation.

Equation (3) is the Poisson equation (elliptic PDE) that relates the current inside the heart to the extracellular electrical potential. Time does not appear explicitly in the Poisson equation and it must be solved simultaneously with Eq. (2) at every time step. The term I_{ext} allows for the introduction of external current as it happens during a defibrillation event.

In the present study, we use the three-dimensional geometry corresponding to the rabbit heart ventricles [6].

To solve Equations (1–3), appropriate boundary conditions are imposed. These boundary conditions express the current conservation condition at the boundaries.

2.2. Membrane models

From a dynamical point of view, the heart is an excitable medium. This means that a perturbation that overcomes a certain threshold produces an action potential (nonlinear response) that propagates as a wave throughout the entire domain with a characteristic shape and velocity.

Since the 1960s, many differential-equations-based models to describe the kinetics of the cell membrane have been developed. In some cases, models have evolved to become quite complex by representing cellular processes in detail. For example, the Iyer et al. model of a human ventricular cell [7] and the Sampson et al. model of a human Purkinje cell [8] use 67 and 82 variables, respectively, to model intracellular ion concentrations and transmembrane currents that make up action potentials in the underlying systems.

Other models, like the three-variable Fenton and Karma model [9], represent quite faithfully the propagation of the action potential without the numerical burden associated with the large numbers of variables in the more complex models. In 2004, Cherry and Fenton [10] improved the previous model by Fenton-Karma by adding a fourth variable to provide more flexibility in accounting for action potential shape. In 2010, Cantalapiedra et al. [11, 12] developed a five-variable model containing a specific formulation for the transient outward K^+ current, which is important in describing action potentials associated with the Brugada syndrome. In this work, we use a reduced version of the Cantalapiedra et al. model [11, 12] given in the Appendix.

2.3. Computation

To solve Eqs. (1–3) numerically, it is necessary to discretize space and time. For the spatial discretization, the finite-volume method is used [4]. This method is preferred because it conserves exactly the charges moving from a reference volume to the next. The time discretization uses a simple forward-Euler method that parallelizes easily.

The most costly part of the computation comes from the Poisson equation Eq. (3), which we solve using the PETSc package [3]. The spatial discretization of the equation leads to a system of the form

$$Ax = b, \tag{4}$$

where A is a large sparse positive semi-definite constant matrix and the vector x contains the unknowns ϕ_e of every discretized volume of the system.

We tested three different iterative methods: biconjugate gradient stabilized (BCG–STAB), conjugate gradient (CG), and generalized minimum residual (GMRES). All are based on Krylov subspace methods. These methods use projection processes onto Krylov-subspaces to get an approximate solution at every step of the iterative process [13]. We verified the numerical consistency of our results by changing the spatial discretization Δx and the time steps δt. For the three-dimensional simulations, we chose $\Delta x = 0.02$ cm and $\delta t = 0.02$ ($\delta t = 0.002$ during the shock) ms, which is a good trade-off between accuracy and CPU cost.
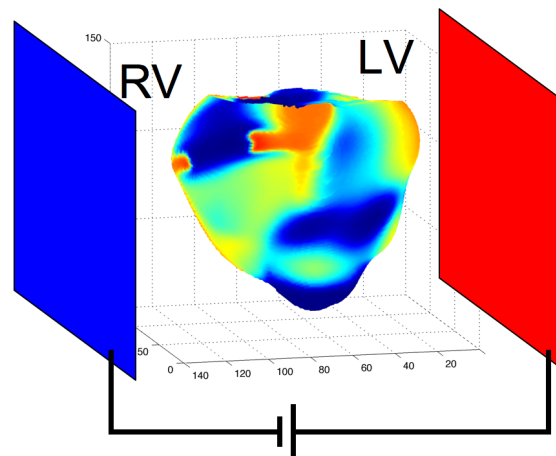
3. Results

Figure 1.   Setup used in this study for quantifying defibrillation efficacy. The electrical activity prior to the shock is highly disorganized. The two acting electrodes are also shown.

The main objective of the present study is to quantify the efficacy of defibrillatory shocks at various energies using our numerical model. We use the rabbit ventricular anatomical model [6] in conjunction with the membrane model detailed in the Appendix. The parameter of the

membrane model are selected to produce a disorganized electrical state corresponding to VF, as shown in Fig. 1.

We simulated the model for 3 s, as shown in Fig. 2. During this time the full dynamical state of the system was saved every 300 ms. These 10 saved states were then used as 10 uncorrelated initial conditions for testing the defibrillation procedure. Indeed, we verified that the absolute value of the Pearson correlation coefficient between any two fields was below 0.2, which indicates that they are uncorrelated. The conventional medical procedure for de-
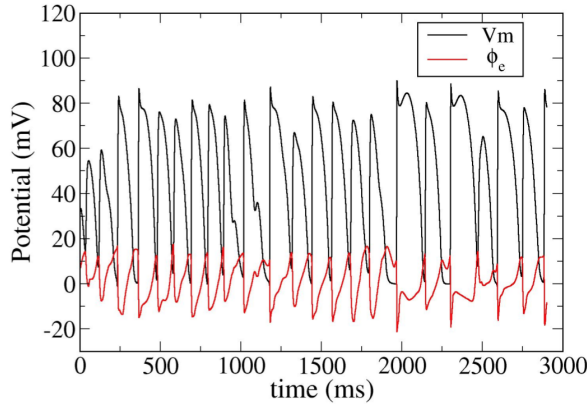

Figure 2. Time evolution of the membrane potential V_m and the extracellular potential (ϕ_e) measured in the middle of the ventricular septum. Note that V_m is given in dimensional units (mV) and has been rescaled and shifted for plotting purposes so that the resting state is 0 mV.

fibrillation consists of applying a very strong electric field through two electrodes placed on the patient torso. In our numerical model, two plane electrodes are placed at the limits of the cubic integration domain in the extracellular region, with the load anode (injecting positive charge) located close to the left ventricle (LV) and the load cathode located close to the right ventricle (RV), as depicted in Fig. 1.

Figure 3 shows the evolution of wave dynamics in response to a successful defibrillatory shock. The shock is applied when sustained fibrillatory dynamics are present. Application of the shock quickly results in strong polarized activity. The shock results in areas of hyperpolarization and depolarization. The shock is successful because ultimately electrical activity is extinguished and the ventricles return to a state of quiescence.

Using this setup, we set out to validate our model by comparing the shock strength needed for successful defibrillation with published data. Here, we used monophasic shocks 12 ms in duration. Five levels of shock intensity were tested corresponding to inter-electrode electric field strengths of 3.6, 7.25, 10.87, 14.5, and 18.12 V/cm. Using the 10 different initial conditions, we calculated statistics
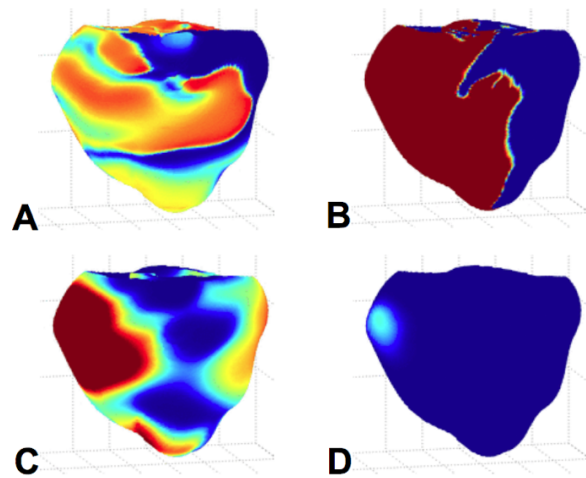

Figure 3. Four snapshots during successful defibrillation using a monophasic shock of 12 ms duration. A) Electrical activity before the shock. B) Strong polarized activity during the shock. C) Activity 50 ms after the end of the shock. D) No activity 100 ms after the end of the shock.

for the success rate. After the 12-ms shock was applied, the system evolved for 600 ms. Then the outcome of the numerical experiment was classified as follows. If the activity stopped directly, it was considered a success (score 1). If disorganized activity remained after 600 ms, it was considered a failure (score 0). If only a single beat (ectopic beat) was observed, it was scored at 0.5. The results of all the simulations are shown in Fig. 4. The analysis of the results can be made using the well-known dose-response curve [14], which is defined as follows:
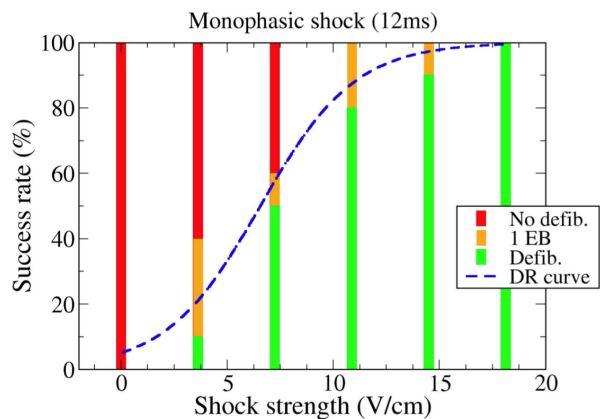

Figure 4. Defibrillation success rate as a function of electrical shock strength as obtained through the 50 numerical simulations. The dashed curve (dose-response curve) represents the best fit of the data through Eq.5. EB: extra beat. DR: dose-response.

$$P(I) = \frac{1}{1 + \exp[k(I_{50} - I)]} \tag{5}$$

where P indicates the probability of success as a function of the dose intensity I.

A direct fit of the curve given by (Eq.5) using the data of Fig.4 results in the following values: $I_{50} = 6.6$ (V/cm) and $k = 0.45$ (cm/V). This means that a shock with an electric field above 6.6 V/cm would provide a 50% chance of efficacious defibrillation. The latter is in good agreement with values found in the medical literature [15].

4.   Conclusions

In this study we developed a parallel numerical code to simulate the electrical activity of the heart and applied the code to study defibrillation. We found that the shock strength needed to defibrillate the numerical heart agrees well with what has been reported experimentally and clinically [15]. Our next step is optimize our defibrillation protocol using additional numerical simulations. Our objective is to reduce the energy content of the shock, thereby lowering the risk of irreversible tissue damage. Energy reductions are expected to result from optimizing such parameters as electrode positions and polarity; number, duration, and frequency of shocks; and shock waveform.

Acknowledgements

References

[1]   Efimov I, Kroll M, Tchou P. Cardiac Bioelectric Therapy. Springer, New York, 2009.

[2]   Trayanova N, Constantino J, Ashihara T, Plank G. Modeling Defibrillation of the Heart: Approaches and Insights. IEEE Reviews in Biomedical Engineering 2011;4:89–102.

[3]   Balay S, Buschelman K, Eijkhout V, Gropp W, Kaushik D, Knepley M, McInnes L, Smith B, Zhang H. In PETSc Users Manual. Argonne National Laboratory; 2008.

[4]   Sachse F. Computational Cardiology. Springer, Berlin-Heidelberg, 2004.

[5]   Aguel F, Eason J, Trayanova N. Advances in modeling cardiac defibrillation. IJBC 2003;13(12):3791–3803.

[6]   Vetter F, McCulloch A. Three-dimensional analysis of regional cardiac function. Prog in Bioph Mol Biology 1998; 69(2):157–183.

[7]   Iyer V, Mazhari R, Winslow RL. A computational model of the human left-ventricular epicardial myocyte. Biophys J 2004;87(3):1507–1525.

[8]   Sampson K, Iyer V, Marks A, Kass R. A computational model of Purkinje fibre single cell electrophysiology : implications for the long QT syndrome. J Physiol 2010; 588:2643–2655.

[9]   Fenton F, Karma A. Vortex dynamics in three-dimensional continuous myocardium with fiber rotation: Filament instability and fibrillation. Chaos 1998;8(1):20–47.

[10] Cherry E, Fenton F. Suppression of alternans and conduction blocks despite steep APD restitution: electrotonic, memory, and conduction velocity restitution effects. Am J Physiol Heart Circ 2004;286):H2332–H2341.

[11] Cantalapiedra I, Peñaranda A, Echebarria B, Bragard J. Phase-2 reentry in cardiac tissue: Role of the slow calcium pulse. Phys Rev E 2010;82(1)):1907.

[12] Peñaranda A, Cantalapiedra I, Bragard J, Echebarria B. Cardiac dynamics: A simplified model for action potential propagation. Theo Biol and Med Modelling 2012;9:50.

[13] Saad Y. Iterative Methods for Sparse Linear System. Springer-Verlag, New York, 2002.

[14] Stroobandt R, Barold S, Sinnaeve A. Implantable cardioverter-defibrillators step by step. Wiley-Blackwell, Chichester, 2009.

[15] Wharton J, M. Wolf P, Smith W, Chen P, Frazier D, Yabe S, Danieley N, Ideker R. Cardiac potential and potential gradient fields generated by single, combined, and sequential shocks during ventricular defibrillation. Circulation 1992; 85:1510–1523.

Appendix

Below we give the detailed formulations of the transmembrane currents $I_m = J_{fi} + J_{si} + J_{so} + J_{to}$ used in this study. The membrane potential V is written in dimensionless form and is re-scaled in the range $[0, 1]$.

$$J_{fi} = -g_{fi}\, s\, (V - V_c)\, (V_{fi} - V)\Theta(V - V_c)\,, \tag{6}$$

$$J_{si} = -g_{si}\, w\, \{1 + \tanh[\beta_1(V - V_1)]\} \{1 + \tanh[\beta_2(1 - V)]\}\Theta(V - V_c)\,, \tag{7}$$

$$J_{so} = g_{so}\left\{\frac{V}{V_c}[1 - \Theta(V - V_c)] + \Theta(V - V_c)\right\} \tag{8}$$

$$J_{to} = g_{ito}\, r\, s\, V\,, \tag{9}$$

where $\Theta(x)$ is the usual Heaviside function and where the dynamics for the three ionic gate variables are as follows:

$$\frac{\partial s}{\partial t} = \frac{\Theta(V_c - V) - r}{\tau_{s_1} + (\tau_{s_2} - \tau_{s_1})\Theta(V_c - V)} \tag{10}$$

$$\frac{\partial r}{\partial t} = \frac{\Theta(V - V_r) - r}{\tau_{r_1} + (\tau_{r_2} - \tau_{r_1})\Theta(V - V_r)} \tag{11}$$

$$\frac{\partial w}{\partial t} = \frac{\Theta(V_c - V) - w}{\tau_{w_1} + (\tau_{w_2} - \tau_{w_1})\Theta(V_c - V)} \tag{12}$$

The time constants τ that appear in Eqs. (10–12) are fitted to reproduce specific characteristics of heart tissue, such as the action potential duration (APD) and conduction velocity (CV) restitution curves, as well as action potential (AP) shapes.